JOURNAL OF SOLID STATE CHEMISTRY **133,** 59–67 (1997)
ARTICLE NO. SC977309

Syntheses, Crystal Structures, and Electronic Structure of the Boron Halides B_9X_9 (X = Cl, Br, I)

Wolfgang Hönle, Yuri Grin, Armin Burkhardt, Ulrich Wedig, Martin Schultheiss, and Hans Georg von Schnering

Max-Planck-Institut für Festkörperforschung, Heisenbergstrasse 1, D-70569 Stuttgart, Germany

and

Ralf Kellner and Herbert Binder

Institut für Anorganische Chemie der Universität, Pfaffenwaldring 55, D-70569 Stuttgart, Germany

Received January 21, 1997; accepted February 6, 1997

The crystal structures of B_9Cl_9 and B_9Br_9 have been determined with X-ray single crystal structure analysis (subcell: $R\bar{3}m$ (166); $Z = 6$; $a = 1259.6(5)$ pm, $c = 1700.1(5)$ pm (B_9Cl_9); $a = 1317.5(3)$ pm, $c = 1777.6(3)$ pm (B_9Br_9)). Both compounds are isotypic and consist of a tricapped trigonal B_9 prism (C_{3v}) with different bond lengths for the triangles (180.0 pm; 176.5 pm), edges (205.7 pm; 201.0 pm), and caps (174.0 pm; 173.5 pm). For better understanding of the bonding in these clusters the electronic structures of the nonaboranes(9), the dianion $B_9Br_9^{2-}$, $B_8Cl_8^{2-}$, $H_2B_9Br_9$ (three types), and $B_{10}H_{14}$ have been calculated and compared with respect to their bond distances and configurations together with the experimental results. The calculation of the Electron Localization Function (ELF) of these molecules and anions shows that the 2*e*–3*c* bonds play a dominant role in these polyhedral cages. The changes in bonding going from the *non-Wade* cluster B_9Br_9 with 18 cluster electrons to the *Wade* cluster $B_9Br_9^{2-}$ with 20 cluster electrons can be visualized by the ELF.

INTRODUCTION

The chemistry of polyhedral boron halides has been reviewed recently in an excellent paper (1). In the course of our research program, $B_{10}H_{14}$ was found to undergo a cluster degradation reaction. By this, we were able to synthesize in good yield the boron monohalides B_9Cl_9 and B_9Br_9, which allowed us to determine the crystal structures as well as to perform chemical reactions (2) leading to interesting new compounds. For a better understanding of the bonding in these halides and related ones, quantum chemical calculations together with the electron localization function were undertaken.

SYNTHESES

The preparation of the monohalides is carried out either in a sealed quartz ampoule (B_9Cl_9),

$$B_{10}H_{14} + \frac{26}{6}C_2Cl_6 \rightarrow \frac{26}{3}C + 14HCl + BCl_3 + B_9Cl_9, \quad [1]$$

or in an autoclave (B_9Br_9) with teflon insert,

$$B_{10}H_{14} + 13\ Br_2, l \rightarrow 14HBr + BBr_3 + B_9Br_9. \quad [2]$$

$B_{10}H_{14}$ undergoes a cluster degradation reaction with elemental bromine at 200°C or with C_2Cl_6. The obtained yield (not optimized) is 40%.

The chloride is extracted with pentane or CH_2Cl_2, filtered by a G4 frit, and concentrated. Sublimation in sealed quartz ampoules at 80°C and $p_{sub} = 10^{-3}$ Torr yields yellow-orange needles.

The bromide is obtained by direct sublimation out of the mixture in an evacuated ampoule in the form of ruby red crystals ($T_{sub} = 200$°C, $p_{sub} = 10^{-3}$ Torr).

All handling of the monohalides is performed in an argon-filled glove box equipped with a microscope. Selected single crystals are transferred into glass capillaries and fixed with baked-out silicon grease, followed by sealing of the capillaries inside the box.

X-RAY CRYSTAL STRUCTURE DETERMINATIONS

Precession photographs with Mo$K\alpha$ radiation are used to check the crystal quality and the symmetry. The intensities

0022-4596/97 $25.00

TABLE 1
Crystallographic Details of B_9Cl_9 and B_9Br_9

Formula	B_9Cl_9	B_9Br_9
Molecular weight [a.m.u.]	416.37	816.43
Space group (No.); Z	$R\bar{3}m$ (166); $Z = 6$	$R\bar{3}m$ (166); $Z = 6$
Lattice constants [pm]	$a = 1259.6(5)$	$a = 1317.5(3)$
of the subcell at (295 K)	$c = 1700.1(5)$ pm	$c = 1777.6(3)$ pm
Volume [$\times 10^{-6}$ pm^{-3}]	2335.99	2672.18
$N(hkl)$ measured	1378	4948
$N(hkl)$ unique	681	460
Variables	51	53
$R(F)$; $R_w(F^2)$	0.0395; 0.153	0.0442; 0.114

of suitable single crystals are measured with an automated four-circle diffractometer (STOE Stadi 4). The crystal structures were solved with SHELXS and refined with SHELXL-93 [3]. Crystallographic details are given in Table 1; the positional and displacement parameters are given in Table 2.

Both structures show a superstructure (subscript s) with $a_s = a$ and $c_s = 3c$. The crystal structure of B_9Cl_9 already described earlier [4] was perhaps given with incorrect symmetry. The corresponding lattice constants can be transformed easily by the matrix (subscript o for the old setting): space group $A2/m$, $a_o = 925$ pm, $b_o = 1266$ pm, $c_o = 1350$ pm, $\beta_o = 95.1^\circ$ [$a = 0.33a_o - 0.33b_o - 0.33c_o$; $b = a_o + b_o$; $c = 0.33a_o - 0.33b_o + 0.67c_o$].

TABLE 2
Positional and Displacement Parameters for B_9Cl_9 and B_9Br_9 in the Subcell

Atom	Site	x	y	z	U_{eq}
			B_9Cl_9		
Cl1	18 h	0.2042(1)	$x/2$	0.86295(8)	790(5)
Cl2	18 h	0.4618(1)	$x/2$	0.74164(9)	904(6)
Cl3a[a]	36 i	0.3721(6)	0.2060(14)	0.0573(4)	977(63)
Cl3b[a]	36 i	0.3570(5)	0.1494(9)	0.0592(3)	581(26)
B1	18 h	0.956(5)	$x/2$	0.7875(3)	458(13)
B2	18 h	0.5714(5)	$x/2$	0.6671(3)	475(13)
B3	18 h	0.5203(5)	$x/2$	0.0594(3)	524(15)
			B_9Br_9		
Br1	18 h	0.2043(2)	$x/2$	0.8638(1)	759(7)
Br2	18 h	0.4617(2)	$x/2$	0.7419(1)	852(7)
Br3a[b]	36 i	0.3717(6)	0.2097(9)	0.0580(4)	693(57)
Br3b[b]	36 i	0.3551(6)	0.1456(12)	0.0601(4)	643(39)
B1	18 h	0.0892(16)	$x/2$	0.7839(9)	490(50)
B2	18 h	0.5786(14)	$x/2$	0.6631(9)	475(49)
B3	18 h	0.5255(15)	$x/2$	0.0599(11)	488(54)

Note. The U_{eq} values are given in pm^2 (standard deviations in parentheses).

[a] SOF = 0.496(6) and (1 − SOF).

[b] SOF = 0.499(6) and (1 − SOF).

The origin of the superstructure is not yet clear. The anisotropy of the observed U_{ij} values, however, indicates that a split description of at least the equatorial halogen atoms may be more adequate for the description of the subcell. Therefore Table 2 gives this split position for the atoms X3.

Both molecules are tricapped trigonal prisms with the symmetry C_{3v}, neglecting the split positions (Fig. 1). The polyhedral cluster B_9 is a *closo* borane with $2n = 18$ cluster electrons, but does not obey Wade's rules for such systems. Figure 1 gives a schematic view of the tricapped trigonal prism. In Fig. 2 a plot of the displacement parameters displaying the split positions of the equatorially bonded halogen atoms is drawn. The skeletal boron atoms also show some indications of the split, however, due to the small differences between split and nonsplit refinements, the improvement of the reliability factors is not significant with the split description of the skeletal boron atoms in that stage of refinement.

Quantum chemical calculations (details see below) with the symmetry C_3 were performed to check whether the calculated energies would give a hint as to the most stable configuration. However, calculations with B_9Br_9 and the restriction to C_3 always relax to D_{3h}.

The reduction of B_9Br_9 with Nbu_4I [2] in CH_2Cl_2 yields the solvated salt $(Nbu_4)_2B_9Br_9 \cdot CH_2Cl_2$ containing the dianion $B_9Br_9^{2-}$ as a *closo*-Wade cluster with $2n + 2 = 20$ electrons. The changes in bond lengths are dramatically large. The observed sequence in bond lengths $B > A > C$ is typical for this kind of neutral clusters. The dianion, however, shows the different sequence $A > B > C$, indicating an enlarged amount of electron localization between the two axial triangles and the presence of strong $2e$–$3c$ bonds with maxima above the triangular faces of the caps. The reduction enlarges bond type A and reduces bond type B by 20 pm; also, type C is reduced by 7 pm. The exocyclic bonds

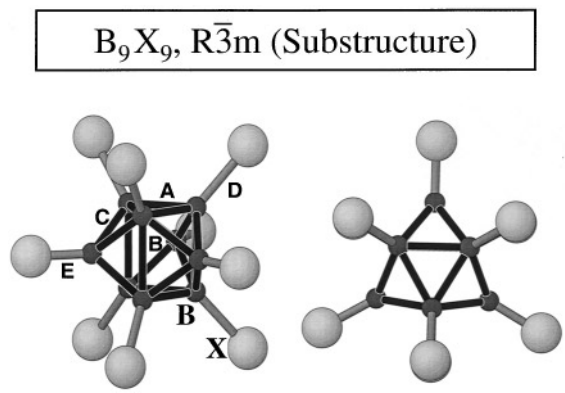

FIG. 1. Left: Schematic view of the tricapped trigonal prism B_9X_9 together with the labels of the mean bond types (cf. Table 3 for the individual values). Right: View along the threefold axis.

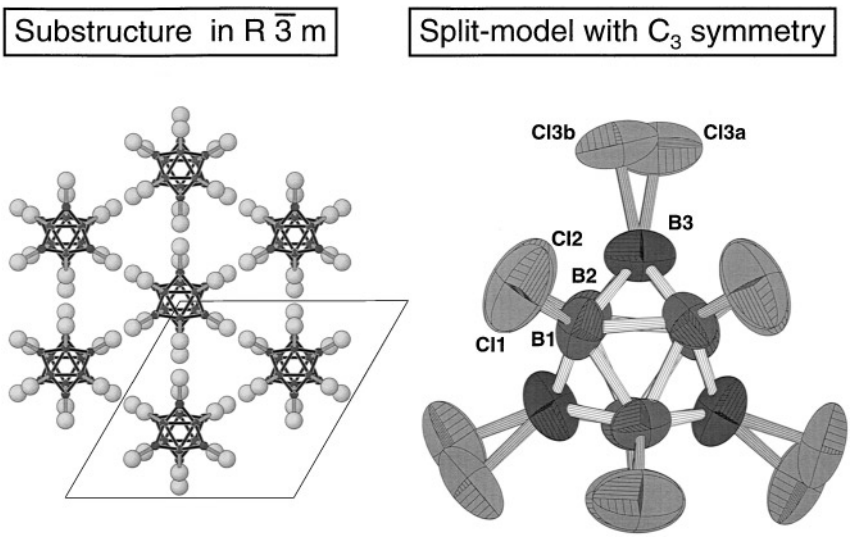

FIG. 2. Left: Parallel view along the crystallographic c-axis into the rhombohedral subcell of B_9X_9. The gravicenters of the molecules in the positions (xyz) are (0, 0, 0), (2/3, 1/3, 1/3), and (1/3, 2/3, 2/3). Right: View along the threefold axis of the split model of B_9Cl_9 with anisotropic displacement parameters (50% probability).

to the halogen atoms are enlarged by 10 pm. Table 3 gives a compilation of the experimentally observed and calculated bond lengths, as obtained by quantum chemical calculations the details of which are given below.

The calculated (D_{3h}) and observed bond lengths of the substructure agree better than those described earlier (5). Their differences indicate, that the calculation method, used here, is reliable enough to predict also details of the unknown members of the cluster series. Up to now we were not able to perform a single crystal X-ray study of a compound containing the $B_9X_9^{1-}$ cluster. Several trials fail and we think, that the expected properties (reactivity) of such a radicalic anion prevent its isolation in the solid state. From experiments in solution, however, there are well defined results, showing that the monoanion exists (2).

INVESTIGATION OF $H_2B_9Br_9$

For better understanding of the electronic structures, we were interested also in the structure of the molecule $H_2B_9Br_9$, because the skeleton is isoelectronic with $B_9Br_9^{2-}$. Up to now there has been no experimental result for the crystal structure of $H_2B_9Br_9$. However, due to the reliable results obtained with the 18e systems, we performed also quantum chemical calculations for the 20e systems.

In principle there are many possible sites for the bonding of the hydrogen atoms. We have chosen three possibilities, named type I, II, and III. For the calculation the symmetry was restricted to C_{2v}. In type I the H atoms are positioned above an axial edge of the trigonal prism. Type II is the

TABLE 3
Comparison of Experimental (X-ray) Averaged Bond Lengths and Calculated (calc.) Values for B_9X_9 (X = Cl, Br, I) and the Dianion $B_9Br_9^{2-}$

Compound	Method	A [pm]	B [pm]	C [pm]	D [pm]	E [pm]
B_9Cl_9	X-ray	180.0	205.7	174.0	174.7	170.9
B_9Cl_9	calc.	182.0	205.0	175.3	174.7	171.2
B_9Cl_9	X-ray (5)	183.4	207.2	176.7	176.5	173.4
B_9Br_9	X-ray	176.5	201.0	173.5	193.3	188.6
B_9Br_9	calc.	181.9	204.0	175.5	190.9	187.0
$B_9Br_9^{2-}$	X-ray[a]	196.0	178.0	167.0	196.0	198.0
$B_9Br_9^{2-}$	calc.	199.6	178.0	169.5	196.5	196.3
B_9I_9	clac.	182.0	203.2	176.0	213.7	209.3

Note. For the labels A–E see Fig. 1.
[a] In $(Nbu_4)_2B_9Br_9 \cdot CH_2Cl_2$(in $P\bar{1}$).

TABLE 4
Calculated Bond Lengths in B_9Br_9, $B_9Br_9^{2-}$, and in the Three Types (I, II, III) of $H_2B_9Br_9$

Compound	A [pm]	B [pm]	C [pm]	D [pm]	E [pm]	H [pm]
B_9Br_9	181.9	204.0	175.5	190.9	187.0	
$B_9Br_9^{2-}$	199.6	178.0	169.5	196.5	196.3	
$H_2B_9Br_9$-I	171.6	282.7	217.6	192.8	190.1	144.4
edge	168.7	258.2	189.0	189.4	189.5	140.9
			172.2			
$H_2B_9Br_9$-II	225.9	173.7	176.2	189.8	190.6	142.3
top triangle						
$H_2B_9Br_9$-III	197.8	200.7	184.5	192.6	192.6	153.8
cap	185.8	197.9	175.1	190.4	191.0	125.7
			173.1			

Note. The bond type H gives the bond lengths of the different hydrogen atoms. The multiplicity of the bond types is not given here.

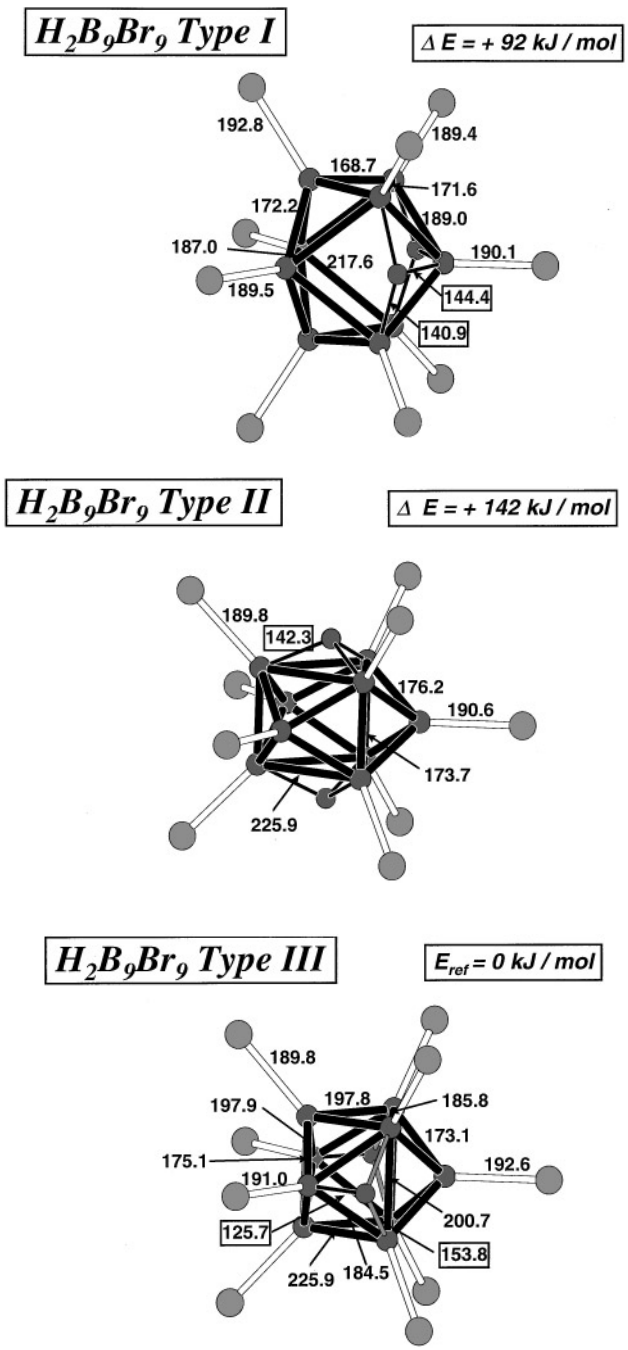

FIG. 3. $H_2B_9Br_9$ molecules as a result of quantum chemical calculations. The averaged bond lengths are given in the figure together with the H atoms (halogen atoms: large spheres; boron atoms: medium spheres; hydrogen atoms: small spheres). Note the three different positions of the hydrogen atoms above the edges [Type I], above the triangular axial faces [Type II], and above the triangular faces of the caps [Type III]. The relative energies are given also in the figure.

most symmetrical one, namely the H atoms are on the threefold axis, capping the triangular axial top and bottom cap. In type III the hydrogen atom is placed above an triangular face formed by the capping atoms of the squaric face.

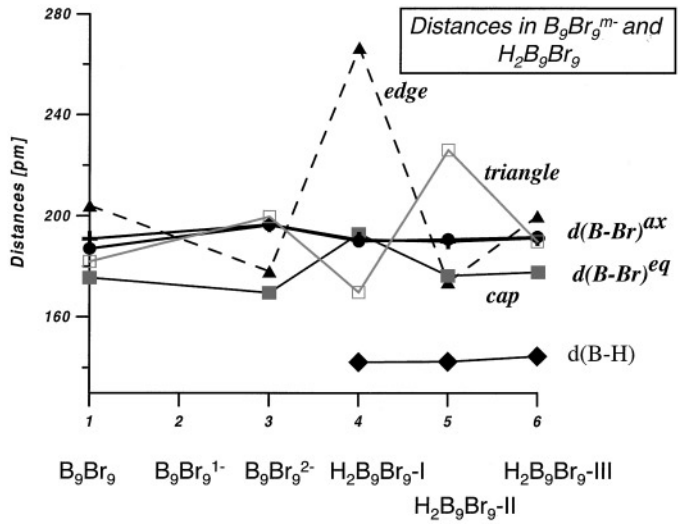

FIG. 4. Distances in the boron clusters $B_9Br_9^{m-}$ ($m = 0, 1, 2$) and in the three models of $H_2B_9Br_9$. The three main bonding types in the clusters are symbolized with different symbols. The distances to the axial (ax) and equatorial (eq) boron atoms are given, too.

The results of the calculations in terms of bond lengths and energies are given in Table 4 and Fig. 3.

The calculated energies are given in Fig. 3. Type III with the hydrogen atoms on the triangular faces has the lowest

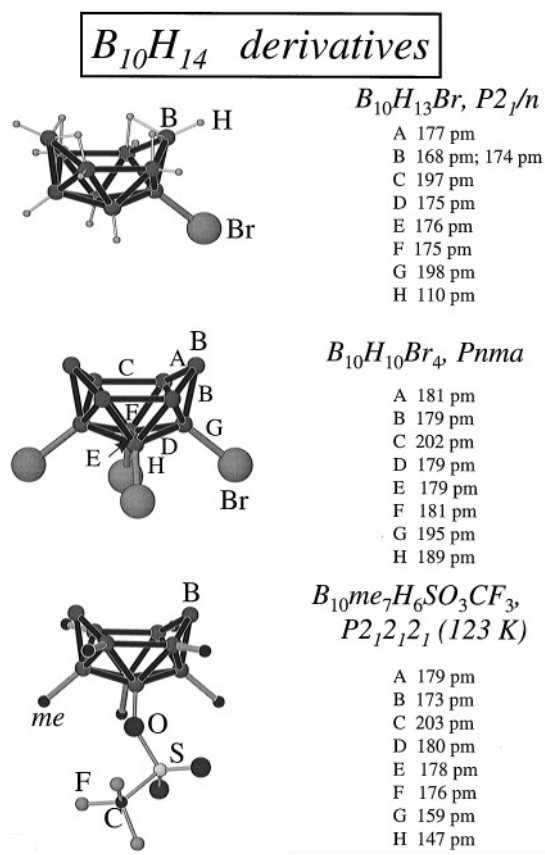

FIG. 5. Three substituted $B_{10}H_{14}$ derivatives together with the main bond lengths. For the labels see the central molecule.

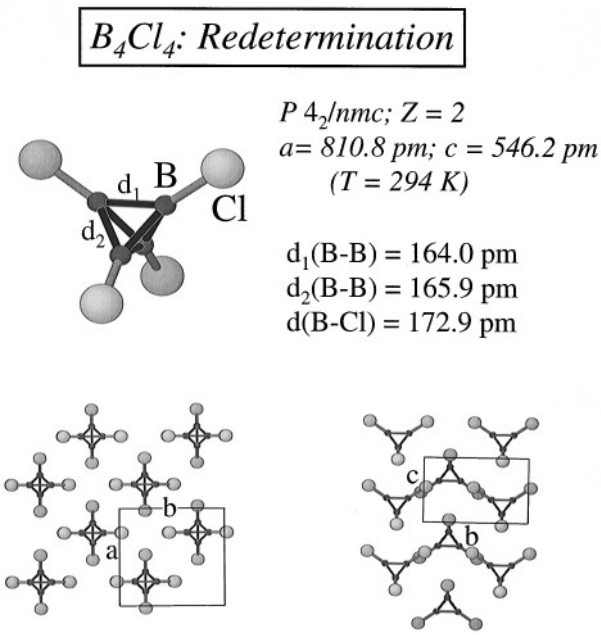

FIG. 6. Results of the redetermination of the crystal structure of B_4Cl_4 together with two projections.

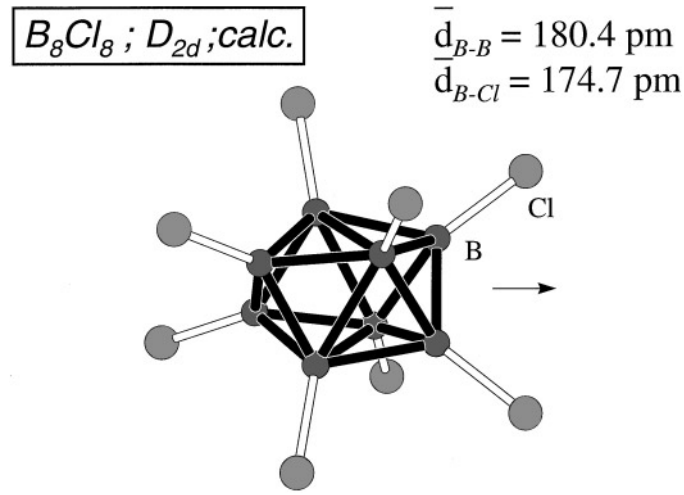

FIG. 7. Calculated structure of B_8Cl_8 with D_{2d} symmetry. The arrow indicates the twofold axis.

THE CLUSTERS B_4Cl_4, B_8Cl_8, AND DERIVATIVES OF $B_{10}H_{14}$

The new preparation method, applied here, allows for the determination of the crystal structures of several derivatives of the $B_{10}H_{14}$ skeleton. Some examples are given in Fig. 5 together with the main bond lengths of the B_{10} cluster. The bond lengths show small but distinctive changes upon substitution. The details of these crystal structures will be published elsewhere.

Due to our knowledge in the preparation of air sensitive compounds, we were able to redetermine the crystal structure of B_4Cl_4 (6). The results allow for a comparison between experimental and quantum chemical results (7). Figure 6 gives the main details of the redetermination together with bond lengths and the two main projections. Figure 7 shows the results obtained from the quantum chemical calculations for B_8Cl_8 with D_{2d} symmetry.

We have also calculated the parent cluster $B_{10}H_{14}$, the results of which are given together with the other clusters below.

QUANTUM CHEMICAL CALCULATIONS

All quantum chemical calculations have been performed with the programme system TURBOMOLE 89 (8) using a DZP basis set (9) and the pseudopotentials developed at

energy, we choose this configuration as the reference. The less stable configuration is type II, although there is a small local minimum at the optimized position. A medium stable structure with respect to the reference is type II. The calculated averaged bond lengths d(B–H) are within the range of observed bond lengths for such types of bonds, but the individual values show a broad range and indicate that in the case of type III there is only one strong bond d(B–H) = 125.7 pm. The two other bonds are much weaker and proof, that the bridging position indeed is an covalently bonded H atom with only one single bond.

More instructive than the individual bond lengths are the changes of each type with the kind of molecule itself. Figure 4 gives the distances according to their function. The most stable Type III has in general nearly the same range of distances as the dianion, but note the interplay between edge, triangle, and cap. Type I, which is the medium stable molecule, shows strong deviations from the known range of distances, whereas Type II might be more stable when changing the kind of halide (Cl or I). Figure 4 also allows for an extrapolation for the unknown details of $B_9Br_9^{1-}$ together with Tables 3 and 4.

FIG. 8. (a) B_4H_4 and (b) B_4Cl_4. Note the extended ELF isosurface of B_4H_4 as compared with B_4Cl_4, due to the strong electron draw of the halogen atoms. The blue color corresponds here to ELF = 0.80, due to an older representation. The isosurfaces around the hydrogen atoms have been clipped to allow for the visibility of the H atom. (c) $B_6H_6^{2-}$ (ELF = 0.80) and (d) $B_8Cl_8^{2-}$(ELF = 0.85). Note the dual polyhedron of the octahedron (cube) and the isolated isosurfaces of the dianion $B_8Cl_8^{2-}$ not leading to an convex polyhedron. (e) View of $B_{10}H_{14}$ directly into the *nido* cluster (ELF = 0.85). (f) $B_{12}H_{12}^{2-}$ (ELF = 0.80) with the dual polyhedron of an icosahedron, which itself is an icosahedron. The isosurfaces of the hydrogen atoms have been clipped to allow for the visibility of the hydrogen atoms. (g) Another view of the B_{10} cluster showing the localization above an edge (ELF = 0.85). (h) Side view of the B_{10} cluster with a $2e$–$3c$ bond maximum located above a triangular face (ELF = 0.85).

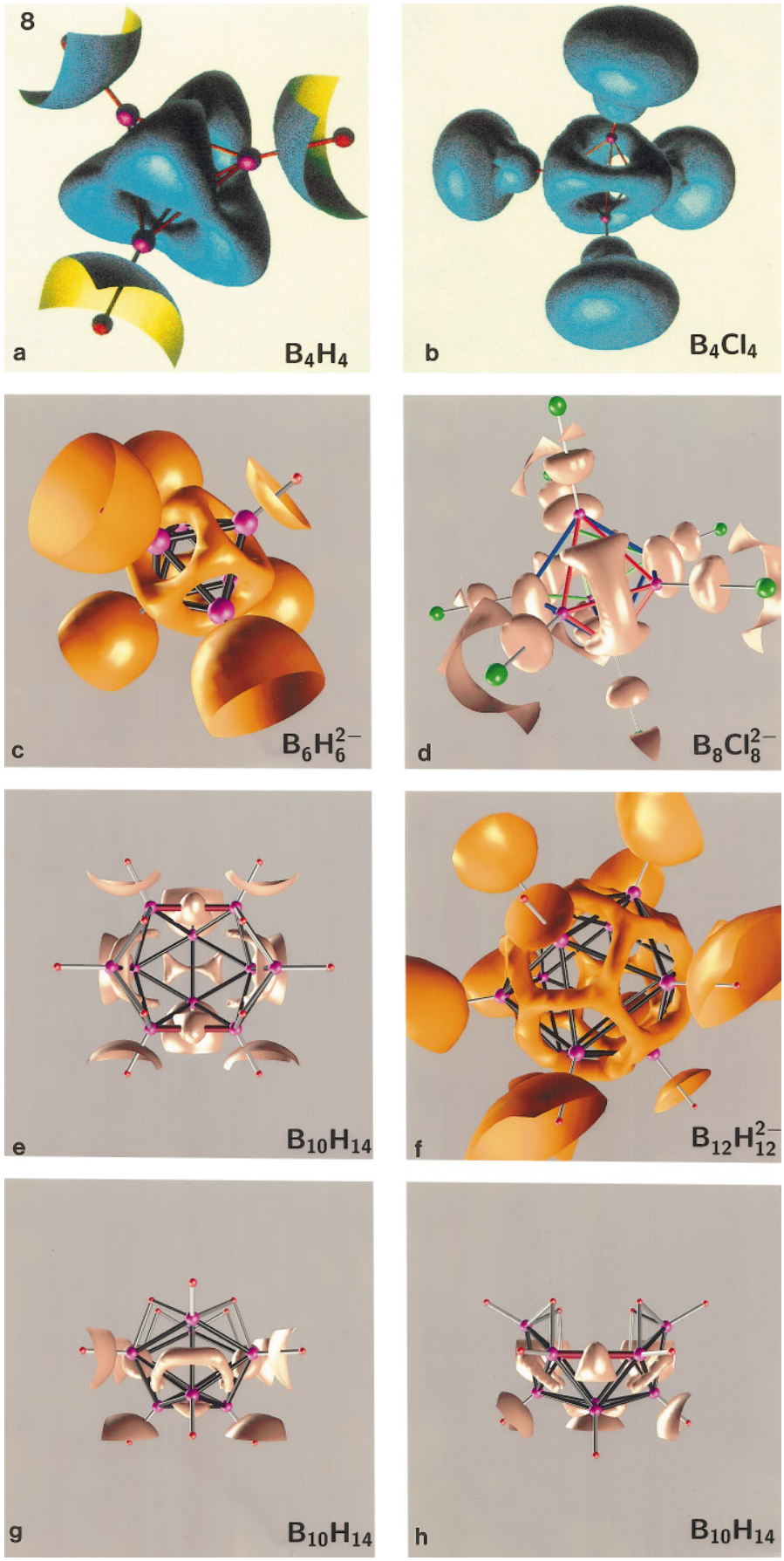
8
a
B_4H_4
b
B_4Cl_4
c
$B_6H_6^{2-}$
d
$B_8Cl_8^{2-}$
e
$B_{10}H_{14}$
f
$B_{12}H_{12}^{2-}$
g
$B_{10}H_{14}$
h
$B_{10}H_{14}$

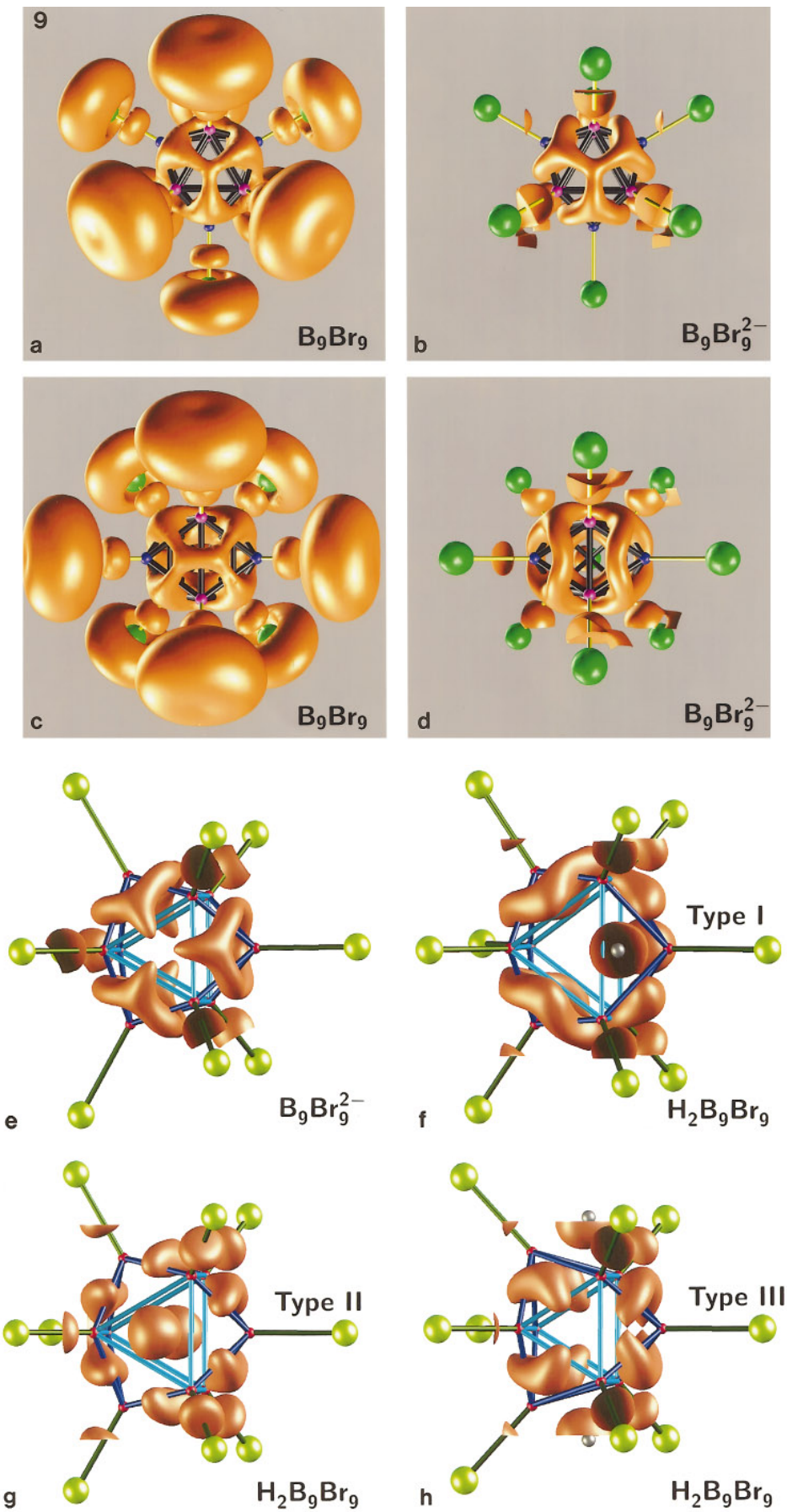
9
a
B_9Br_9
b
$B_9Br_9^{2-}$
c
B_9Br_9
d
$B_9Br_9^{2-}$
e
$B_9Br_9^{2-}$
f
Type I
$H_2B_9Br_9$
g
Type II
$H_2B_9Br_9$
h
Type III
$H_2B_9Br_9$

the University of Stuttgart (10). The calculation of B_4H_4, B_4Cl_4, $B_6H_6^{2-}$, and $B_8Cl_8^{2-}$, as well as $B_{12}H_{12}^{2-}$, was performed using the highest possible point symmetry. For the compounds B_9X_9 the symmetries D_{3h}, C_{3v}, and C_3 were considered. In the cases of $B_9Br_9^{2-}$ and $H_2B_9Br_9$ the point symmetries D_{3h} and C_{2v} were applied, respectively.

THE ELECTRON LOCALIZATION FUNCTION (ELF) AS A TOOL FOR VISUALIZATION OF BONDING

The Electron Localization Function (ELF) has been proved [11] to give appreciable insight into the bonding of molecules, clusters, and solids, not only for covalent compounds, but also for intermetallic compounds [12]. It is suitable also for systems with high symmetry and multicenter bonding. The ELF has values close to *unity* in regions of covalent bonds, lone pairs, or core shells, and it is close to *zero* in regions "between shells." A color code based on a map is used to indicate high values as white (snow-covered mountains) and low values as blue (deep oceans). The ELF isosurfaces for the figures given here fall into the range $0.80 \leq \text{ELF} \leq 0.85$, thus allowing a visual comparison of the electronic characteristics for a $2n$ and $(2n + 2)$ electron cluster. Figures 8 and 9 represent the ELF isosurfaces of different boron clusters. We have included also for the purpose of comparison some "old friends," namely B_4H_4, B_4Cl_4, $B_6H_6^{2-}$, and $B_{12}H_{12}^{2-}$.

In B_9Br_9, as in the other *closo* boranes (7), the maxima of ELF form the dual polyhedron of the boron cage (Fig. 8, Figs. 9a, c). Adding two additional electrons to the cluster reduces the ELF at the edges of the trigonal prism (cf. Fig. 9d versus Fig. 9c). The electron localization is more structured, being more prominent on the faces of the caps. The three caps seem to be the dominant structural element less tightly coupled to form the whole cluster. This results in shorter distances C and longer distances A (cf. Table 3). The shortening of B is due to the contraction of the caps and not caused by a stronger B–B bonding along the edges.

For $H_2B_9Br_9$ three local minima for the energy surface were investigated. In the most stable structure (III), the proton is bonded to the capping boron atom. ELF indicates a B–H single bond to be present. However, further calculations (molecular dynamics) have to be performed to allow for a more final interpretation of this compound.

TABLE 5
Calculated Averaged Bond Distances d(B–B) and d(B–X) for Different Boron Clusters

$B_nX_n^{m-}$ $n = 4, 6, 8, 9, 12$ $m = 0, 2$	d(B–B) [pm]	d(B–X) [pm]
B_4H_4	167.9	118.7
B_4Cl_4	168.3	172.7
B_4Br_4	168.0	187.7
B_4I_4	167.8	209.6
$B_6H_6^{2-}$	172.9	122.5
$B_6Cl_6^{2-}$	170.1	183.6
$B_6Br_6^{2-}$	170.1	197.9
$B_6I_6^{2-}$	170.1	218.8
B_8Cl_8	180.4	174.7
B_9Cl_9	181.5	173.5
B_9Br_9	181.4	189.6
$B_9Br_9^{2-}$	179.3	196.4
$H_2B_9Br_9$-III	184.2	191.3
B_9I_9	181.6	212.2
$B_{12}H_{12}^{2-}$	178.0	120.9

It is an old but nevertheless still interesting question how the boron–boron distances depend upon the cluster size. This question has already been partially answered recently (7). Table 5 gives averaged calculated bond lengths of different boron clusters together with the corresponding values of distances to the substituents H or X. This compilation shows that at one hand there is a general trend of increasing bond lengths d(B–B) as a function of cluster size, coinciding with the shorter distances of the ELF maxima from the polyhedral faces of the cages. On the other hand, there are still open questions to be answered by new calculations and experiments.

OUTLOOK

Due to the new synthetic routes and availability of the monohalides, one can expect new experimental results. The

FIG. 9. (a, b) View parallel to the threefold axis upon the axial triangle of B_9Br_9 (a) and $B_9Br_9^{2-}$ (b) (for both, ELF = 0.80). Note the changes of the maxima above the triangular faces of the axial caps as well as of the triangular cap to the equatorial halogen atoms. In (b) the isosurfaces of the halogen atoms have been clipped. The localization of bonding electrons in the bond direction B–Br is also noteworthy (a). (c, d) View perpendicular to the threefold axis showing the maxima above the edges of the neutral cluster (c) and the dianion (d). (e) Comparative view (ELF = 0.83) of $B_9Br_9^{2-}$ and the three types of $H_2B_9Br_9$. The trigonal prismatic skeleton is given with light blue bonds, the bonds to the capping boron atoms are drawn in dark blue color. The boron atoms are represented as small red spheres, the bromide anions are shown green, whereas the hydrogen atoms are given with silver color. The ELF isosurfaces of the lone pairs of the halogen atoms as well as those for the bonds from boron to bromine have been partially clipped for better visibility. Note the changes of the maximum above the axial triangular cap in going from (d) (ELF = 0.80) to (e) (ELF = 0.83). (f) $H_2B_9Br_9$, Type I, with the hydrogen atoms located above the edges of the trigonal prism. (h) $H_2B_9Br_9$, Type III, as the most stable configuration of the calculated models. Note the changes in the maxima in the vicinity of the hydrogen atoms as compared with (e). (g) gives the less stable configuration of $H_2B_9Br_9$, Type II, with the hydrogen atoms located above the axial triangular cap. Also, the maxima above the triangular faces of the capping atoms have been minimized by the hydrogen atoms.

integration of electron density and the transformation into more simple pictures together with improved calculations will allow for a better understanding of the relationship between structure, bonding and reactivity.

ACKNOWLEDGMENTS

The competent help of Dr. Jürgen Nuß (MPI) with plotting and drawing is gratefully acknowledged. Thanks are also due to the Fonds der Chemischen Industrie for financial support.

REFERENCES

1. J. A. Morrison, *Chem. Rev.* **91,** 35 (1991).
2. R. Kellner, N. Berger, R. Stöckle, K. Vaas, S. Söylemez, A. Pfitzner, H. Binder, W. Hönle, Y. Grin, A. Burkhardt, M. Schultheiss, U. Wedig, H. G. von Schnering, H. Borrmann, and A. Simon, "Advances in Boron Chemistry, IX. International Meeting on Boron Chemistry," July 14–18, 1996, University of Heidelberg, Collected Abstracts, p. 70, Session Lecture SA-6.
3. G. M. Sheldrick, SHELXS 86, University of Göttingen, 1986; G. M. Sheldrick, SHELX-L 93, University of Göttingen 1993.
4. M. B. Hursthouse, J. Kane, and A. G. Massey, *Nature* **228,** 659 (1970).
5. D. J. Swanton, R. Ahlrichs, and M. Häser, *Chem. Phys. Lett.* **155,** 329 (1989).
6. W. Einholz, "Advances in Boron Chemistry, IX. International Meeting on Boron Chemistry," July 14–18, 1996, University of Heidelberg, Collected Abstracts, p. 80, Session Lecture CA-22.
7. A. Burkhardt, U. Wedig, H.G. von Schnering, and A. Savin, *Z. Anorg. Allg. Chem.* **619,** 437 (1993).
8. R. Ahlrichs, M. Bär, M. Häser, H. Horn, and C. Kölmel, *Chem. Phys. Lett.* **162,** 165 (1989).
9. G. Igel-Mann and H. J. Poppe, personal communication.
10. G. Igel-Mann, H. Stoll, and H. Preuß, *Mol. Phys.* **65,** 1321 (1988).
11. A. D. Becke and K. E. Edgecombe, *J. Chem. Phys.* **92,** 5397 (1990); A. Savin, A. D. Becke, J. Flad, R. Nesper, and H. G. von Schnering, *Angew. Chem.* **103,** 421 (1991); *Angew. Chem. Int. Ed. Engl.* **30,** 409 (1991).
12. Y. Grin, U. Wedig, and H. G. von Schnering, *Angew. Chem.* **107,** 1318 (1995); *Angew. Chem. Int. Ed. Engl.* **34,** 1204 (1995).